Shanmugasundaram and Lee
Micro and Nano Systems Letters (2022) 10:13
https://doi.org/10.1186/s40486-022-00154-7

Micro and Nano Systems Letters

LETTER Open Access

SnO_2/rGO nanocomposite for the detection of biomarkers of lung cancer

Arunkumar Shanmugasundaram[1,3] and Dong-Weon Lee[1,2,3*]

Abstract

Metal oxide-based sensors have been widely used to detection biomarkers in exhaled breath for identification of various diseases such as asthma, diabetes, halitosis, and lung cancer. Herein, we proposed one step hydrothermal method for the preparation of SnO_2 nanospheres and reduced graphene oxide incorporated SnO_2 nanospheres for the detection of two important biomarkers such as decane and heptane from the exhaled breath of lung cancer patients. The as prepared materials are investigated in detail through various analytical techniques and the findings are consistent with each other. The sensing response of the proposed sensors were systematically investigated to enhance their sensing performance as a function of operating temperatures and gas concentration, and different analyte gases. The sensors showed maximum sensing response toward heptane and decane compared to other interfering gases such as hydrogen, carbon monoxide, acetone, ethanol, and methanol at 125 °C. The proposed sensors exhibit excellent detection range as low as 1 ppm with appreciably fast response and recovery time. Lung cancer patients may be easily screened using the proposed sensor, by detecting decane and heptane in their exhaled breath.

Keywords: Gas sensor, SnO_2/rGO hybrid nanocomposite, Heptane and decane sensing, High sensitivity, Excellent selectivity

Introduction

According to the World Health Organization (WHO), lung cancer is one of the leading cause of deaths in both men and women. Therefore, the detection and diagnosis of lung cancer at early stage is important to save millions of people life. Over the years techniques have been proposed such X-ray, computed tomography (CT) scan, and magnetic resonance imaging (MRI). Despite their high accuracy, these approaches are not immediately adaptable to routine lung cancer screening and early detection due to their high cost. Additionally, these approaches need skilled personnel to operate and investigate. Recently, several non-radiative techniques have been proposed among them, detection of biomarkers in exhaled breath considered as an effective technique for early diagnosis of lung cancer.

Recently several techniques have been proposed for the detection of biomarkers in exhaled breath such as chromatography-mass spectroscopy [1], infrared spectroscopy [2], opto-chemical fibers [3], ion flow tube mass spectrometry [4], surface acoustic wave sensors [5]. Nonetheless, these breath analysis systems are not readily portable, are often costly, and have a somewhat long reaction time. To overcome the drawbacks of these techniques, metal oxide-based semiconductors have been used for the detection of biomarkers in exhaled breath owing to its excellent sensing response, fast response, and recovery time. To date, several metal oxide-based gas sensors such as SnO_2 [6, 7]. In_2O_3 [8, 9], ZnO [10, 11], Fe_3O_4 [12], WO_3 [13] have been proposed for the detection of various biomarkers including acetone, formaldehyde, acetaldehyde, heptane, benzene, isoprene, styrene, methanol, ethanol, toluene, xylene, n-pentane, heptane, propanol, isopropanol, cyclohexane, cyclopentane,

*Correspondence: mems@jnu.ac.kr

[1] MEMS and Nanotechnology Laboratory, School of Mechanical Engineering, Chonnam National University, Gwangju 61186, Republic of Korea
Full list of author information is available at the end of the article

n-decane, and ammonia are associated with the lungs [14]. However, the concentration of these biomarkers in the exhaled breath are too low sometime in ppb level. Thus, the detection of these biomarkers in the exhaled breath remains challenge for the researchers. Therefore, an effective, and efficient biosensing platform to detect the lung cancer biomarkers is highly desired to save millions of human's lives.

Herein, we propose one step hydrothermal method to preparation of SnO_2 nanospheres and reduced graphene oxide incorporated SnO_2 nanocomposite for the detection of heptane and decane in the exhaled breath. The proposed sensor showed maximum sensing response toward decane, and heptane compared to other interfering gases at 125 °C. The reduced graphene oxide incorporated SnO_2 nanocomposite sensor can detect decane and heptane as low as 1 ppm with the response (15 s, 19 s) and recovery time (90 s, 48 s) and remarkable selectivity at the optimal working temperature of 125 °C, which makes it possible for real-time detection of decane and heptane biomarkers in exhaled breath.

Experimental section

Chemicals

Graphite flakes (+100 mesh), potassium permanganate ($KMnO_4$), sulfuric acid (H_2SO_4), hydrochloric acid (HCl), hydrogen peroxide (H_2O_2), tin (II) chloride ($SnCl_2{\cdot}2H_2O$), urea (CH_4N_2O), ethanol (C_2H_5OH), were purchased from Sigma-Aldrich Chemical Co. All chemicals were of analytical reagent (AR) grade and used as received.

Preparation of SnO_2 nanospheres

In a typical synthesis procedure calculated amount of tin (II) chloride was dispersed in distilled (DI) water followed by the addition of urea under constant magnetic stirring. After 60 min of stirring, ethanol was added into the above solution to get the desired reaction mixture. After 3 h of vigorous stirring, the solution was poured into a stainless-steel autoclave and kept inside the programmable oven at 120 °C. After 24 h of hydrothermal, the autoclave was cooled down to room temperature naturally and the precipitate formed at the bottom of the autoclave was collected and centrifuged to remove the residual impurities. Then, the material was dried at 70 °C for 12 h.

Preparation of reduced graphene oxide incorporated SnO_2 nanocomposite

The preparation of graphene oxide (GO) is described in detail in Additional file 1. In a typical synthesis procedure of Reduced graphene oxide incorporated SnO_2 nanocomposite, firstly calculated amount of tin (II) chloride was dispersed in a DI water. Then, calculated amount of GO was ultrasonically dispersed in the above solution. After 30 min of ultrasonication, urea was added to solution followed by the addition of ethanol. The solution mixture was then transferred into the Teflon-lined stainless-steel autoclave and kept in a programable oven at 120 °C and maintained at that temperature for 24 h. The autoclave was naturally cooled to room temperature after 24 h of hydrothermal, and the precipitate formed at the bottom of the autoclave was collected and centrifuged to remove any remaining contaminants. The material was then dried for 12 h at 70 °C.

Results and discussion

Details of the experimental methods and characterisation techniques is described in Additional file 1. Powder X-ray diffraction analysis was used to characterize the crystal structure and phase purity of as-prepared SnO_2 nanospheres and Reduced graphene oxide incorporated SnO_2 nanocomposite (Fig. 1). The diffraction patterns of the as-prepared SnO_2 nanospheres and Reduced graphene oxide incorporated SnO_2 nanocomposite are rutile (JCPDS No. 41-1445, a0 = 4.738, c0 = 3.178) [6, 7]. The Reduced graphene oxide incorporated SnO_2 nanocomposite exhibits a similar diffraction pattern to SnO_2 nanospheres. The absence of the reduced graphene oxide diffraction pattern in the Reduced graphene oxide incorporated SnO_2 nanocomposite may be attributable to the composite's low graphene oxide concentration, which beyond the X-ray diffractor's detection limit [15, 16]. No

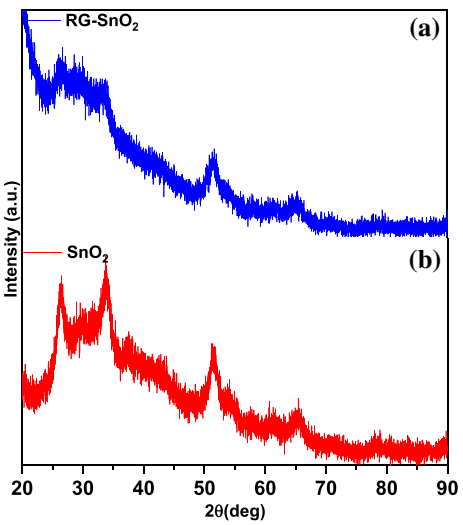

Fig. 1 Crystal structure and phase purity analysis. Powder X-ray diffraction pattern of the as-prepared **a** SnO_2 nanospheres and **b** reduced graphene oxide incorporated SnO_2 nanospheres nanocomposites

other impurity phase was observed indicating the phase pure formation of the as-prepared materials.

The morphologies of the as-prepared materials were characterized by the field emission scanning electron microscope (FESEM) and transmission electron micrograph (TEM) along with high resolution transmission electron micrograph (HRTEM) and selected area electron pattern (SAED) analysis. Figure 2 shows the FESEM images of the as-prepared SnO_2 nanospheres and (c, d) reduced graphene oxide incorporated SnO_2 nanospheres nanocomposites at two different magnifications. Figure 2a, b shows the birds view and closer view of the as-prepared SnO_2 nanospheres. The lower magnified image shows the several nanoparticles of size ~ 50 nm. The higher magnified image reveals hierarchical mesoporous nature of the as-prepared SnO_2 nanospheres. Each of the SnO_2 nanospheres are composed of smaller nanoparticles of size ~ 5 nm. Figure 2c, d shows the FESEM images of the as-prepared reduced graphene oxide incorporated SnO_2 nanospheres nanocomposites at lower and higher magnifications. In the low magnification FESEM image, the presence of smaller SnO_2 nanospheres evenly dispersed across the RGO sheets is clear. The higher magnification FESEM image demonstrates the formation of a hybrid nanocomposite comprising SnO_2 nanospheres and rGO nanosheets.

TEM was used to further clarify the morphology of the as-prepared Reduced graphene oxide incorporated SnO_2 nanocomposite. As seen in Fig. 3a, the Reduced graphene oxide incorporated SnO_2 has a sheet-like structure with some curvatures. The rGO nanosheets contains many ultrafine SnO_2 nanospheres that are homogeneously scattered. Numerous darker nanoparticles were observed in the low magnified TEM image,

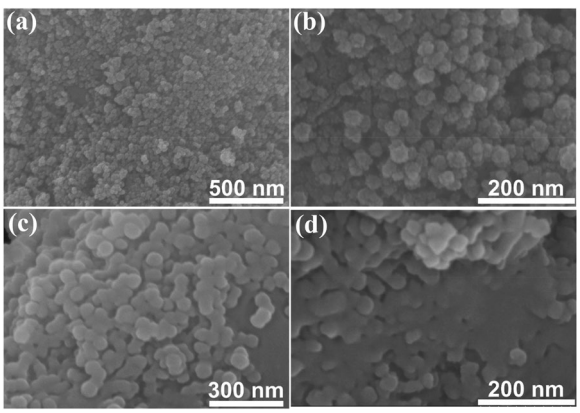

Fig. 2 Electron microscopy images of the as-prepared materials in scanning mode. **a**, **b** FESEM images of the SnO_2 nanospheres and **c**, **d** reduced graphene oxide incorporated SnO_2 nanospheres nanocomposites at two different magnifications

indicating that SnO_2 nanospheres attached on both sides of rGO nanosheets. The higher magnified image shows the lattice fringes with spacing of 0.32 nm corresponding to the (110) plane of the rutile SnO_2 crystal structure. The selected area electron diffraction pattern shows the diffraction rings which can be indexed to the (110), (101), (200), and (211) planes of the rutile SnO_2 crystal structure [6, 7].

The detailed gas sensors fabrication and techniques used for the measurement of sensing response toward analyte gases were described in detail in Additional file 1. Figure 4 shows the dynamic heptane and decane sensing characteristics of the fabricated sensors based on SnO_2 nanospheres and reduced graphene oxide incorporated SnO_2 nanospheres. Figure 4a shows the schematic diagram of the gas sensing measurement system that has been used for the heptane and decane sensing analysis. The proposed pristine SnO_2 nanospheres and reduced graphene oxide-SnO_2 sensors were exposed to heptane and decane for one minute to compare their sensing response. The operating temperature of the sensors where the surface adsorption–oxidation–desorption gas kinetic reactions are optimum were investigated by measuring the sensing response as a function of temperature to 4 ppm of decane and heptane. Figure 4a shows the temperature-dependent sensing characteristics of the sensors to 4 ppm of heptane and decane. The sensing response of the sensors were increased with increasing operating temperature. All the fabricated sensors were showed maximum sensing response towards decane and heptane at 125 °C. The maximum sensing response of the sensors based on SnO_2 nanospheres and rGO incorporated SnO_2 nanospheres at 125 °C toward 4 ppm of decane and heptane was found to be ~ 28.27, and 59.10, respectively.

The activation energy of the sensing materials is another important factor which determine the sensing performance of the sensors. The activation energy can be described as the minimum energy that is required to take out the electron from the sensor response. The activation energy of the sensing materials can be calculated using Arrhenius equation [15, 16].

$$S = S_0 exp\left(\frac{E_g}{2K_B T}\right), \tag{1}$$

where S, S_0, K_B, T, and E_g are the sensor response, pre-exponential factor, Boltzmann constant, thermodynamic temperature, and activation energy, respectively.

The calculated activation energy of the sensors based on SnO_2 nanospheres and Reduced graphene oxide incorporated SnO_2 nanocomposite toward decane and heptane was found to be ~ 0.34 eV, 0.32 eV, and 0.22 eV

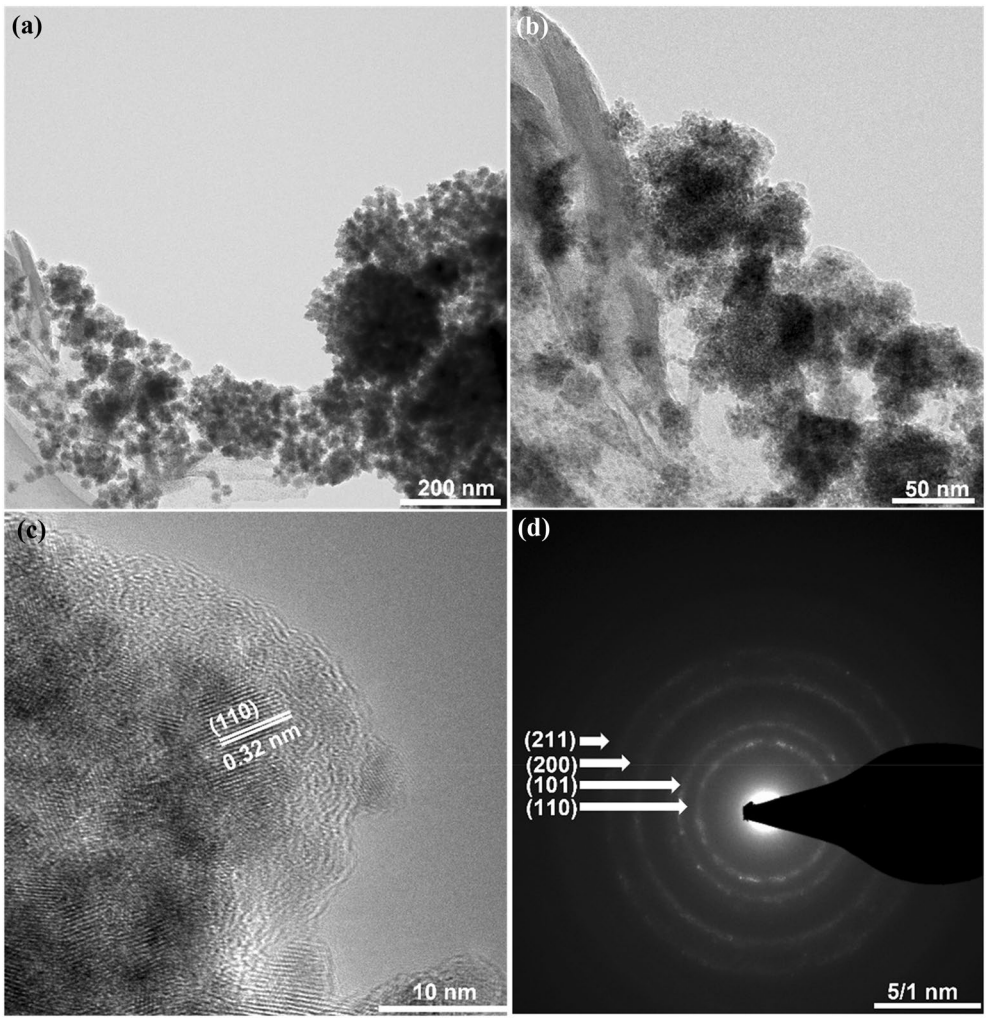

Fig. 3 Electron microscopy images of the as-prepared materials in transmission mode. **a**, **b** TEM images of the reduced graphene oxide incorporated SnO_2 nanospheres nanocomposites at two different magnifications. **c** High-resolution transmission scanning electron micrograph of the as prepared reduced graphene oxide incorporated SnO_2 nanospheres nanocomposites. **d** Selected area electron diffraction pattern of the as-prepared reduced graphene oxide incorporated SnO_2 nanospheres nanocomposites

and 0.19 eV, respectively. The minimum activation energy of the Reduced graphene oxide incorporated SnO_2 sensor toward heptane indicating the improved sensing performance of the sensors toward heptane. Figure 4c, d shows the dynamic sensing characteristics and sensing response of the sensor based on Reduced graphene oxide incorporated SnO_2 nanocomposite as a function of different decane concentrations ranging from 1 to 4 ppm at 125 °C. The sensing response of the sensors increased with increasing the gas concentration. Besides, the sensing response increased with increasing gas concentration then saturated and recovered back to its original base resistance once the gas is turned off. The maximum sensing response of the Reduced graphene oxide incorporated SnO_2 nanocomposite sensor for 1, 2, 3, and 4 ppm of decane was found to be ~ 2.72, 3.15, 3.94, 4.56, respectively. Figure 4e, f shows the dynamic sensing characteristics and sensing response of the sensor based on Reduced graphene oxide incorporated SnO_2 nanocomposite toward 1–4 ppm of heptane at 125 °C. The Reduced graphene oxide incorporated SnO_2 nanocomposite sensor exhibits its excellent response and recovery sensing capabilities toward heptane as shown in Fig. 4e. The base response resistance of the sensors increased with the gas concentration and saturated then came back to its original resistance value once the gas turned off. The sensing response of the Reduced graphene oxide incorporated

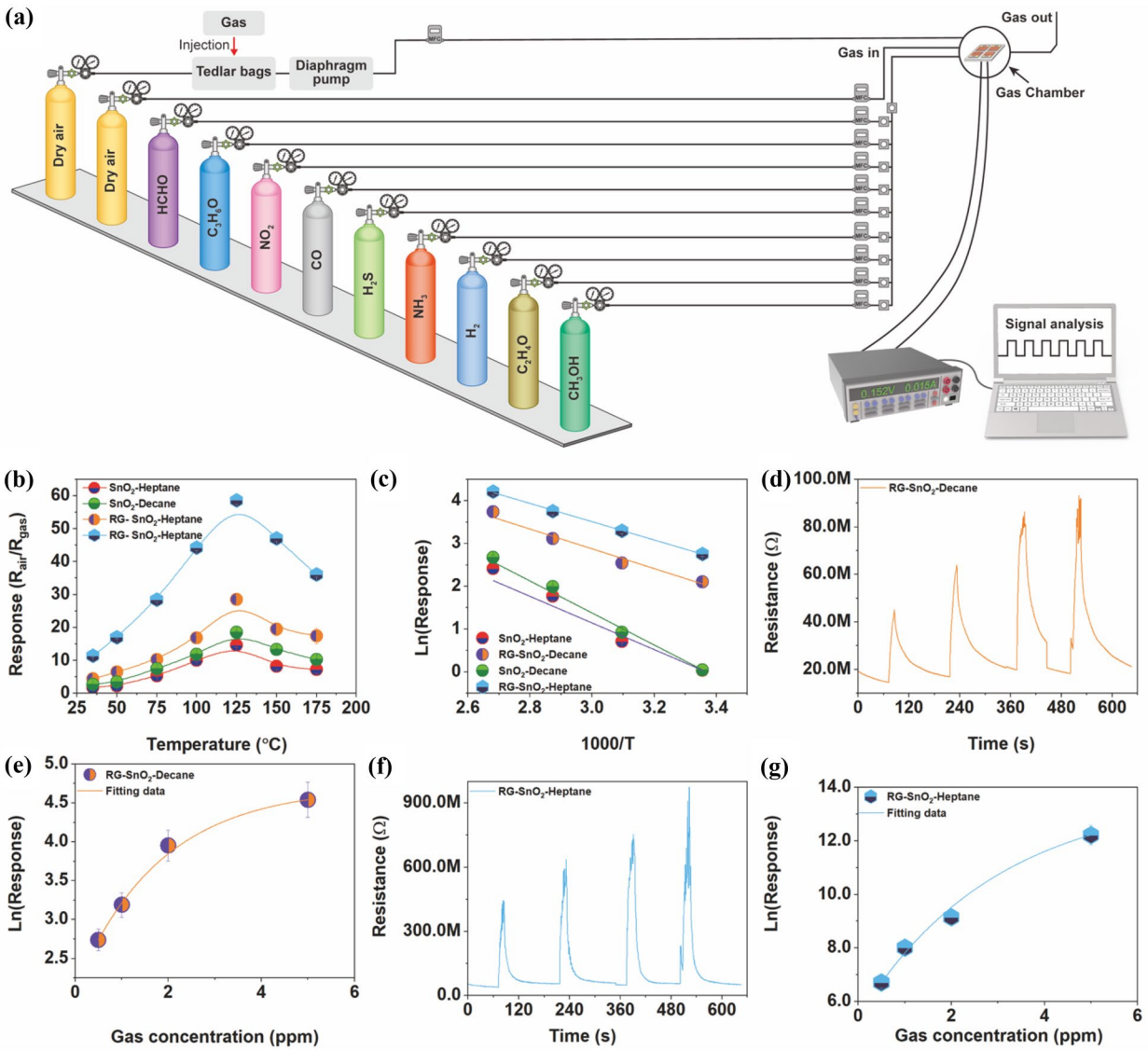

Fig. 4 Heptane and decane sensing characteristics of the sensors based on SnO_2 nanospheres and reduced graphene oxide incorporated SnO_2 nanospheres. **a** Schematic diagram of the gas sensing measurement system. **b** Temperature-dependent sensing characteristics of the sensors to 4 ppm of heptane and decane and **c** corresponding Arrhenius sensing response of the sensors. **d**, **f** Dynamic heptane and decane sensing characteristics of the sensors based on SnO_2 nanospheres and reduced graphene oxide incorporated SnO_2 nanospheres at 125 °C to 1–4 ppm. **e**, **g** Corresponding sensing response of the sensor as a function decane and heptane concentration at 125 °C

SnO_2 sensor for 1, 2, 3, and 4 ppm heptane was found to be 6.63, 8.03, 9.24, and 12.31, respectively. Although the Reduced graphene oxide incorporated SnO_2 nanocomposite sensor could detect both decane and heptane at 125 °C, the sensing response of the sensor toward heptane is ~ 3 times higher compared to that of the sensing response of the sensor toward decane.

Figure 5a, b shows the response and recovery time of the sensor based on Reduced graphene oxide incorporated SnO_2 nanocomposite toward 4 ppm of decane and heptane at 125 °C. The response and recovery time of the sensor based on Reduced graphene oxide incorporated SnO_2 nanocomposite toward 4 ppm of decane at 125 °C was found to be 15 and 90 s, respectively. Whereas the response and recovery time of the Reduced graphene oxide incorporated SnO_2 nanocomposite sensor toward 4 ppm of heptane at 125 °C was found to be 19 s and 48 s, respectively. The repeatability and long-term stability of the sensor are the imperative factors that determines the practical feasibility of

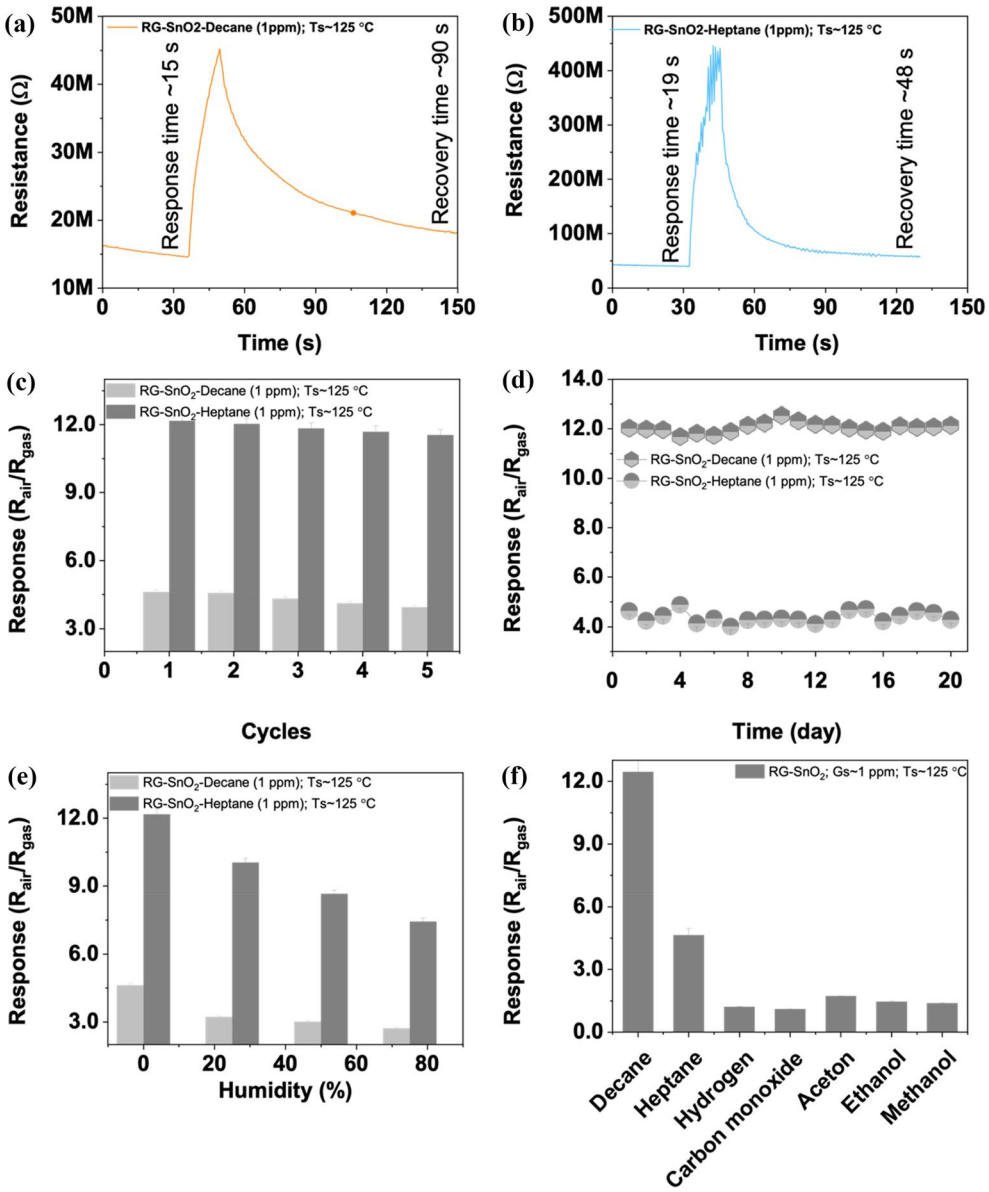

Fig. 5 **a**, **b** Response and recovery time of the sensors based on reduced graphene oxide incorporated SnO_2 nanospheres to 4 ppm of decane and decane at 125 °C. **c**, **d** Reproducibility and long-term stability of the sensors based on reduced graphene oxide incorporated SnO_2 nanospheres to 4 ppm of decane and heptane at 125 °C. **e** Effect of humidity on the sensing response of the sensors based on reduced graphene oxide incorporated SnO_2 nanospheres to 4 ppm of decane and heptane at 125 °C to 5 ppm. Selectivity of the fabricated sensor toward different target gas such as heptane, decane, hydrogen, carbon monoxide, acetone, ethanol, and methanol

the proposed sensor. Therefore, repeatability and long-term stability of the proposed sensor were investigated toward 4 ppm of decane and heptane. The sensing response of the Reduced graphene oxide incorporated SnO_2 sensor toward 4 ppm of decane during 1st, 2nd, 3rd, 4th, and 5th cycles was found to be ~4.51, 4.53, 4.28, 4.13, 3.98, respectively. Whereas the sensing response of the Reduced graphene oxide incorporated SnO_2 nanocomposite sensor to 4 ppm of heptane during 1st, 2nd, 3rd, 4th, and 5th cycles was ~12.21, 12.05, 11.91, 11.62, and 11.62, respectively. The deviation of the sensing response of the Reduced graphene oxide incorporated SnO_2 during 5 repetitive cycle was within ±2% indicating the excellent reproducibility of the proposed sensor. As shown in Fig. 5d, the long-term durability of the fabricated sensor based on Reduced

graphene oxide incorporated SnO_2 nanospheres nanocomposite was assessed by measuring the sensor's sensing response toward 4 ppm of decane and heptane for 3 weeks at 125 °C. During the 21-day period, the sensing response values of the Reduced graphene oxide incorporated SnO_2 based sensor were relatively consistent, with fluctuations of less than 2.1%, demonstrating the proposed sensor's good long-term stability toward decan and heptane.

The sensing response of the Reduced graphene oxide incorporated SnO_2 nanocomposite sensor was examined at various relative humidity levels (RH). Figure 5e demonstrates the sensing response of the Reduced graphene oxide incorporated SnO_2 nanocomposite-based sensors at various ambient humidity. The sensor's sensing response reduced as RH increased for both decane and heptane, which might be because the adsorbed water molecules occupied the adsorption sites on the surface, inhibiting oxygen adsorption. The selectivity of the Reduced graphene oxide incorporated SnO_2-nanocomposite sensor was tested in the presence of several other interfering gases such as hydrogen, carbon monoxide, acetone, ethanol, and methanol. The sensor showed highest sensing response toward heptane, compared to other gases. However, the sensing response of the sensor toward decane is significantly higher compared other analyte gases.

Generally, the sensor response of hybrid nanoparticle metal oxides with reduced graphene oxide are categorized into two groups. In the first category, the sensor response is dominated by metal oxide. The gas sensing principle of n-type metal oxide semiconductors like SnO_2 follows chemisorption-charge transfer- and desorption pathway. At elevated operating temperature the oxygen molecules adsorbed on the SnO_2 surface. The surface adsorbed oxygen molecules are then converted into oxygen radicals such as O^-, O^{2-} and O^{2-} by taking the electrons from the SnO_2 conduction band. This led to decreased sensor conductivity thereby generating electron depletion region. The formation of specific oxygen radicals can be explained as follows.

$$O_2(\text{gas}) \rightarrow O_2(\text{ads}), \tag{2}$$

$$O_2(\text{ads}) + e^- \rightarrow O_2^-(\text{ads}), \tag{3}$$

$$O_2^-(\text{ads}) + e^- \rightarrow 2O^-(\text{ads}). \tag{4}$$

When the sensor exposed to volatile organic compounds (VOC) such as heptane and decane, the gas molecules reacted with the chemisorbed oxygen radicals and released the electrons into the conduction band of the sensing material thereby increase the electrical conductivity of the sensor. The sensing response of the sensor can be calculated by measuring the sensor resistance in the presence of gas and in the presence of air. The specific gas kinetic reaction between the analyte and the chemisorbed oxygen radicals are as follows

$$\text{VOC}_{(\text{gas})} + O_x^{n-}(\text{ads}) \Leftrightarrow \text{VOC-O} + ne^-. \tag{5}$$

Even though the chemisorption/desorption of oxygen species is the underlying principle of sensor performance, the amount of surface adsorbed/desorbed oxygen species involved in gas sensing is highly dependent on the capability of the sensing materials. The surface of SnO_2 nanospheres is highly reactive due to their nanoscale size. The surface of the highly reactive SnO_2 nanospheres absorbs more oxygen species and generates many oxygen radicals on its surface, hence accelerating the gas kinetic processes.

In the second category, the role of reduced graphene oxide is more important than that of metal oxides, where the sensor adsorb and react with the analyte gases. It represents that the sensor shows p-type behavior in which the resistance increases in the presence of a reducing gas. Besides, the excellent sensing characteristics of the reduced graphene oxide incorporated SnO_2 nanocomposite sensor toward heptane and decane compared to that of the bare SnO_2 nanospheres could be attributed to the hierarchical mesoporous nature of the SnO_2 nanospheres and the formation heterostructure between the reduced graphene oxide nanosheets and SnO_2 nanospheres. The SnO_2 nanospheres are uniformly distributed on the reduced graphene oxide nanosheets thus heterojunction is formed in the hybrid nanocomposite. When a sensor is exposed to an analyte gas, dissociated gas may preferentially and strongly adsorb at reduced graphene oxide—SnO_2 nanospheres interfaces because these interfaces have high active sites such as vacancies, line defects, and strong electronic interaction between graphene and metal oxides. Under these conditions, the reduced graphene oxide nanosheets acting as electron transporters will accept electrons from the adjacent SnO_2 nanospheres, hence enhancing the sensing response of the sensor [17]. The proposed reduced graphene oxide-SnO_2 nanospheres sensor showed significantly better or comparable sensing performance compared to the reported heptane and decane sensors as shown in Table 1. Additionally, the excellent selectivity of the Reduced graphene oxide incorporated SnO_2 nanocomposite toward heptane and the significant sensing response toward decane remain unknown and need additional investigation.

Table 1 Heptane and decane sensing characteristics of SnO_2/rGO sensor and that of other reported heptane and decane sensors

Sensing material	T_S[a]	G_C[b]	S_R[c]	$\Gamma_{RES}/\Gamma_{REC}$[d]	Ref.
$MnFe_2O_4$ (Decane)	210	72	4.25	NA[e]	Zhang et al. [18]
CuO (Decane)	230	3000	2	20/200	Xia et al. [19]
Au@ZnO (Decane)	400	100	7	30/3	Feng et al. [20]
TiO_2 (Heptane)	RT	3	21.7	5/2780	Saffary et al. [21]
Au-ZnO (Heptane)	360	50	5	30/14	Han et al. [22]
BNQDs-ZnO (Heptane)	370	100	1.6	3/4	Choudhury et al. [23]
Sr-In_2O_3 (Heptane)	200	100	6	NA[e]	Shen et al. [24]
RG-SnO_2 (Decane)	125	1	2.72	15/90	This work
RG-SnO_2 (Heptane)	125	1	12.31	19/48	This work

[a] Sensing temperature

[b] Gas concentration

[c] Sensor response (R_g/R_a or R_a/R_g)

[d] Response and recovery time

[e] Not applicable

Conclusion

In this work, we have prepared rGO incorporated SnO_2 nanospheres through one step hydrothermal strategy for the detection of biomarkers of lung cancers such as decane and heptane. The crystal structure and morphology of the as-prepared materials were thoroughly studied using XRD, FESEM, TEM, HRTEM, and SAED, and the results were consistent. The sensing characteristics of the fabricated sensors based on SnO_2 nanospheres, and Reduced graphene oxide incorporated SnO_2 nanocomposite were investigated toward different analyte gases and the sensor were showed excellent sensing characteristics toward heptane and significant sensing response toward decane at 125 °C compared to other interfering gases. The Reduced graphene oxide incorporated SnO_2 nanocomposite sensor also exhibits appreciably fast response and recovery time toward heptane and decane along with good excellent long-term reliability and stability. The proposed sensor can be used for the easy screening of the lung cancer patient by detecting decane and heptane in their exhaled breath.

Supplementary Information

The online version contains supplementary material available at https://doi.org/10.1186/s40486-022-00154-7.

Additional file 1. The preparation of graphene oxide, details of the experimental methods and characterization techniques and gas sensor fabrication and measurement techniques is described in detail in the supplementary information.

Acknowledgements
Authors are grateful to the National Research Foundation of Korea for the funds received.

Author contributions
AS designed the research, discussed the results with DWL and contributed to writing the manuscript with DWL. Both authors read and approved the final manuscript.

Funding
This work was financially supported by the National Research Foundation of Korea (NRF) grant funded by the Korean government (MSIT) (No. 2020R1A5A8018367) and Basic Science Research Pro-gram through the National Research Foundation of Korea (NRF) funded by the Ministry of Education (No. 2020R1I1A1A01073562).

Availability of data and materials
The datasets supporting the conclusions of this article are included within the article.

Declarations

Ethics approval and consent to participate
Not applicable.

Consent for publication
Not applicable.

Competing interests
The authors declare that they have no competing interests.

Author details
[1]MEMS and Nanotechnology Laboratory, School of Mechanical Engineering, Chonnam National University, Gwangju 61186, Republic of Korea. [2]Center for Next-Generation Sensor Research and Development, Chonnam National University, Gwangju 61186, Republic of Korea. [3]Advanced Medical Device Research Center for Cardiovascular Disease, Chonnam National University, Gwangju 61186, Republic of Korea.

Received: 22 July 2022 Accepted: 25 August 2022
Published online: 16 September 2022

References

1. Gordon SM, Szidon JP, Krotoszynski BK, Gibbons RD, O'Neill HJ (1985) Volatile organic compounds in exhaled air from patients with lung cancer. Clin Chem 31(8):1278–1282
2. Giubileo GM (2002) Diagnostics by laser-based analysis of exhaled breath. Proc SPIE 4762:318–325
3. Kolle C, Gruber W, Trettnak W, Biebernik K, Dolezal C, Reininger F, O'Leary P (1997) Fast optochemical sensor for continuous monitoring of oxygen in breath-gas analysis. Sens Actuators B Chem 38–39:141–149
4. Smith D, Wang T, Sule-Suso J, Spane P, El-Haj A (2003) Quantification of acetaldehyde released by lung cancer cells in vitro using selected ion flow tube mass spectrometry. Rapid Commun Mass Spectrom 17:845–850
5. Groves WA, Zellers ET, Frye GC (1998) Analyzing organic vapors in exhaled breath using a surface acoustic wave sensor array with preconcentration: selection and characterization of the preconcentrator adsorbent. Anal Chim Acta 371:131–143
6. Manjula P, Arunkumar S, Manorama SV (2010) Au/SnO_2 an excellent material for room temperature carbon monoxide sensing. Sens Actuators B Chem 152(2):168–175
7. Shanmugasundaram A, Basak P, Satyanarayana L, Manorama SV (2013) Hierarchical SnO/SnO_2 nanocomposites: formation of in situ p–n junctions and enhanced H_2 sensing. Sens Actuators B Chem 185:265–272
8. Shanmugasundaram A, Basak P, Manorama SV, Krishna B, Sanyadanam S (2015) Hierarchical mesoporous In_2O_3 with enhanced CO sensing and photocatalytic performance: distinct morphologies of $In(OH)_3$ via self-assembly coupled in situ solid–solid transformation. ACS Appl Mater Interfaces 7(14):7679–7689
9. Shanmugasundaram A, Ramireddy B, Basak P, Manorama SV, Sanyadanam S (2014) Hierarchical $In(OH)_3$ as a precursor to mesoporous

In_2O_3 nanocubes: a facile synthesis route, mechanism of self-assembly, and enhanced sensing response toward hydrogen. J Phys Chem C 118(13):6909–6921
10. Arunkumar S, Tianfeng H, Kim Y-B, Choi B, Park SH, Jung S, Lee DW (2017) Au decorated ZnO hierarchical architectures: facile synthesis, tunable morphology and enhanced CO detection at room temperature. Sens Actuators B Chem 243:990–1001
11. Shanmugasundaram A, Kim DS, Chinh ND, Park JJ, Piao Y-J, Kim J, Lee DW (2021) N-/S-dual doped C@ ZnO: an excellent material for highly selective and responsive NO_2 sensing at ambient temperatures. Chem Eng J 421(1):127740
12. Zhang L, Dong B, Xu L, Zhang X, Chen J, Sun X, Xu H, Zhang T, Bai X, Zhang S, Song H (2017) Three-dimensional ordered ZnO–Fe_3O_4 inverse opal gas sensor toward trace concentration acetone detection. Sens Actuators B Chem 252:367–374
13. Shao S, Chen X, Chen Y, Lai M, Che L (2019) Ultrasensitive and highly selective detection of acetone based on Au@WO_3-SnO_2 corrugated nanofibers. App Surf Sci 473:902–911
14. Chatterjee S, Castro M, Feller JF (2013) An e-nose made of carbon nanotube based quantum resistive sensors for the detection of eighteen polar/nonpolar VOC biomarkers of lung cancer. J Mater Chem B 1:4563
15. Shanmugasundaram A, Chinh ND, Jeong Y-J, Hou TF, Kim DS, Kim D, Kim Y-B, Lee DW (2019) Hierarchical nanohybrids of B-and N-codoped graphene/mesoporous NiO nanodisks: an exciting new material for selective sensing of H_2S at near ambient temperature. J Mater Chem A 7(15):9263–9278
16. Shanmugasundaram A, Gundimeda V, Hou TF, Lee DW (2017) Realizing synergy between In_2O_3 nanocubes and nitrogen-doped reduced graphene oxide: an excellent nanocomposite for the selective and sensitive detection of CO at ambient temperatures. ACS Appl Mater Interfaces 9(37):31728–31740
17. Shanmugasundaram A, Manorama SV, Kim D-S, Jeong Y-J, Lee D-W (2022) Toward point-of-care chronic disease management: biomarker detection in exhaled breath using an E-Nose sensor based on rGO/SnO_2 superstructures. Chem Eng J 448:137736
18. Zhang L, Wang G, Yu F, Zhang Y, Ye B-C, Li Y (2018) Facile synthesis of hollow $MnFe_2O_4$ nanoboxes based on galvanic replacement reaction for fast and sensitive VOCs sensor. Sens Actuators B Chem 258:589–596
19. Xia S, Zhu H, Cai H, Zhang J, Yu J, Tang Z (2014) Hydrothermally synthesized CuO based volatile organic compound gas sensor. RSC Adv 4:57975
20. Feng Z, Ma Y, Natarajan V, Zhao Q, Ma X, Zhan J (2018) In-situ generation of highly dispersed Au nanoparticles on porous ZnO nanoplates via ion exchange from hydrozincite for VOCs gas sensing. Sens Actuators B Chem 255:884–890
21. Saffary Y, Christensen CN, Tripathy A, Jeppson M, Carlson K, Mohanty SK (2022) Synthesis of tetracosane functionalized titanium dioxide sensor for detecting heptane as pneumonia breath biomarker. IEEE Sensors 22(16):15724–15732
22. Han X, Sun Y, Feng Z, Zhang G, Chen Z, Zhan J (2016) Au-deposited porous single-crystalline ZnO nanoplates for gas sensing detection of total volatile organic compounds. RSC Adv 6:37750–37756
23. Choudhury SP, Nakate UT (2022) Study of improved VOCs sensing properties of boron nitride quantum dots decorated nanostructured 2D-ZnO material. Ceram Int 48:28935–28941
24. Shen X, Guo L, Zhu G, Xi C, Ji Z, Zhou H (2015) Facile synthesis and gas-sensing performance of Sr- or Fe-doped In_2O_3 hollow sub-microspheres. RSC Adv 5:64228–64234

Publisher's Note